G. Segura, A. Pournaghshband, S.Afshan, E. Mirambell. (2021) Numerical simulation and analysis of stainless steel frames at high temperature. **Engineering Structures, 227, 111446**.

Numerical simulation and analysis of stainless steel frames at high temperature

G. Segura [(1)], A. Pournaghshband [(2)], S. Afshan [(2)*], E. Mirambell [(1)]

[(1)] *Universitat Politècnica de Catalunya, Barcelona, Spain*

[(2)] *University of Southampton, Southampton, UK*

Abstract

This paper presents a numerical modelling study investigating the response of stainless steel two-dimensional frame assemblies at elevated temperature that has not been the subject of detailed investigation to date. Finite elements models which capture the combined effects of material degradation with temperature and the interaction between the individual frame elements are developed and validated. The effect of key behavioural parameters including frame type, i.e. sway and non-sway, degree of utilisation, material grade and heating profile is investigated through an extensive parametric modelling. A new set of performance criteria in terms of limiting deflection and limiting rate of deflection for sway and non-sway frames in fire is established and verified.

Keywords: Stainless steel frame, fire resistance, nonlinear analysis, parametric study, utilisation ratio

1. Introduction

The design for fire requirements of stainless steel structures in existing structural design codes e.g. in [1-3] is based on the resistance of individual elements, where resistance is determined on the basis of the minimum time that the structural members can withstand exposure to the standard ISO-834 fire curve. Failure criteria in terms of either the collapse of the member and limits of deformation and rate of deformation or maximum limiting temperatures are used to carry out individual member design checks. Fire engineering design based on the whole structural system behaviour rather than isolated member response is now universally recognized and employed for multi-storey steel-framed buildings with composite construction and is exploited in the form of performance-based design methods [4-6]. In performance-based fire engineering design, optimized fire protection systems are developed by first conducting a realistic analysis of the structure exposed to fire and then applying the fire protection where it is required, rather than to all the structural elements as is done in prescriptive-based design, to

meet the codified safety requirements. *Clause 4.3* of EN 1993-1-2 [2] on "Advanced Calculation Models" describes the method of structural analysis for performance-based fire resistant design of carbon steel structures.

Since stainless steels are often left without fire protection, for reasons of intrinsic durability and aesthetic appeal particularly, other means of providing fire resistance, e.g. through performance-based design approach, is needed. However, in previous experimental and numerical modelling studies of stainless steel structures in fire, the focus has largely been on the performance and design of individual structural members including beams e.g. [7-9], columns e.g. [10-13] and beam-columns e.g. [14-15]. Recent studies of the elevated temperature performance of restrained stainless steel columns and beams e.g. [16-19] have investigated the more realistic restraints that take place between the individual elements acting within a structural frame. In these studies, the combined effects of the thermally induced strains and stresses due to temperature rise and mechanical actions on the structural response were assessed to better understand the real behaviour of these structures in fire.

Following on from the realization of the many benefits of design based on whole frame behaviour in fire of carbon steel structures and building on the existing body of knowledge on fire performance of stainless steel structures at member level, the current study aims to investigate the global structural behaviour of stainless steel frame assemblies in fire. A numerical modelling investigation studying the structural behavior of stainless steel two-dimensional frames at elevated temperatures, which captures the combined effects of material degradation with temperature and the interaction between the individual frame elements is carried out. Validated thermal and mechanical numerical models capable of simulating, with high predictive accuracy, the full load-deformation history of two-dimensional stainless steel frames at elevated temperature are generated. The effect of key behavioural parameters including frame type, i.e. sway and non-sway, degree of utilisation, material grade and heating profile is investigated through an extensive parametric modelling, the results of which are presented and discussed.

2. Development of FE models and validation

Since there are no published test data on elevated temperature performance of stainless steel frames, results of tests on carbon steel frames, presented in Section 2.1. are first used to validate

the finite element models, as described in Section 2.2, based on which the parametric study models of stainless steel frames in fire, presented in section 3, are developed.

2.1. Experimental results for validation

The results of fire tests on carbon steel frames conducted by Rubert and Schaumann [20] were used for the validation of the numerical models developed herein. The tests included three different frame configurations namely EHR, EGR and ZSR frame series as shown in Figure 1(a)-(c), respectively. The key details of the tested frames, including the loadings and geometries, are reported in Table 1, and are described hereafter. All the EHR and EGR frames were heated completely and uniformly, except for the EGR7 and EGR8 frames, where their beam members were left unheated. For all the ZSR frames, only one bay, as marked in Figure 1(c), were heated. In Table 1, L and h are the frame width (one bay) and height, respectively, f_y is the measured yield stress at room temperature, F_1 and F_2 are the applied point loads, as shown in Figure 1, μ_0 is the degree of utilization and θ is the failure temperature. The degree of utilization μ_0, defined as the ratio of the applied load in the fire situation (i.e. F_1 or F_2) to the load-bearing capacity at room temperature ($F_{1,u}$ or $F_{2,u}$), had a range of 0.34-0.82. The design load-bearing capacity of the frames at room temperature i.e. $F_{1,u}$ and $F_{2,u}$ were determined by Rubert and Schaumann [20] using a second order analysis, taking into account plastification of the cross-sections and geometric non-linearities. The test failure temperature θ was defined in [20] as the temperature at which the beam mid-span deflection reached a limiting maximum value of $L/60$ (mm), where L is the frame width. All the structural members of the tested frames were IPE 80 profile of carbon steel St37 grade. Torsional displacement and out-of-plane deformation of the frame structural elements were precluded by means of suitable restraints at the locations on the frames marked with a cross in Figure 1.

2.2 Description of FE models

The FE analysis package ABAQUS version 2016 [21] was used to develop a sequentially coupled thermal-stress analysis model. It involved a thermal model to determine the temperature field and a stress model to obtain the load-deformation response of the modelled frames under the combined actions of applied loads, maintained at constant level, and increasing temperatures.

The time-temperature distribution in the structural members was determined by conducting a heat transfer analysis. The heat transfer analysis consisted of transferring heat from fire, defined

by the standard ISO-834 [2] fire curve, through heat transfer mechanisms of convection and radiation. Radiation and convection were modelled by defining surface radiation (*SRADIATE) with emissivity coefficient of 0.7 and film condition (*SFILM) with convective heat transfer coefficient of 25 W/m²K, respectively, as specified in EN 1993-1-2 [2]. The EN 1993-1-2 [2] specified values for the thermal material properties of carbon steel, including thermal conductivity, specific heat and coefficient of thermal expansion data were employed.

The 4-noded S4R and DS4 shell elements, from the ABAQUS element library, were employed to create the structural and thermal analyses models, respectively and were used in all numerical simulations. A uniform mesh size of 5mm×5mm was used based on a mesh sensitivity analysis. The stress-strain model for carbon steel provided in EN 1993-1-2 [2] was adopted to describe the elevated temperature behaviour of the material. The EN 1993-1-2 [2] strength and stiffness reduction factors together with the measured room temperature yield stress f_y and Young's modulus E = 210000 N/mm^2 were used to construct stress-strain curves at elevated temperatures. The creep deformations are implicitly accounted for in this stress-strain model [2]. The true stress σ_{true} and true strain ε_{true}, required for modelling of shell elements in ABAQUS, were incorporated into the FE models - these were derived from the engineering stress σ_{nom} and strain ε_{nom} data using the commonly used relationships $\sigma_{true} = \sigma_{nom}(1+\varepsilon_{nom})$ and $\varepsilon_{true} = \ln(1+\varepsilon_{nom}) - \sigma_{true}/E$, where E is the Young's modulus.

Pinned boundary conditions were applied at the frame supports to simulate the test conditions, where all the translational displacement degrees of freedom and the rotational displacement degrees of freedom, apart from rotation about the cross-section major axis, at the column bases were restrained. Rigid body coupling was used at the end cross-sections of the beam and the column members to restrain the degrees of freedom of all the nodes on the cross-sections to that of their corresponding concentric reference point. The beam and column members were connected via rigid body constraints at their ends to provide full continuity.

The measured initial sway imperfection ϕ of the tested frames was 1/600 and the measured bow imperfection e_0 of the beam and column members were L/3000 and h/3000, respectively [20]. The initial out-of-straightness of the beam and column members was modelled with a half sine wave shape and amplitude equal to the measured values. The frame sway out-of-straightness (h/600) was considered sufficiently small and was not modelled in the validation models. The local imperfection of the plates comprising the cross-sections of the members as

well as the residual stresses were not included in the FE models based on similar assumptions in previous numerical modelling studies e.g. [22].

The stress analysis model was carried out in two steps to replicate the anisothermal loading conditions of the tests, where in Step 1, the loads F_1 and F_2 were applied at room temperature and maintained constant throughout Step 2, where the temperature was increased following the time-temperature relationships stored from the thermal analysis model. The general static solver in ABAQUS, which uses the Newton-Raphson root finding method, was used for both Steps 1 and 2 to solve the sequentially coupled thermo-mechanical problem. In Step 2, where the unstable behaviour of steel members at elevated temperatures caused numerical convergence issues, an adaptive automatic stabilization scheme with a constant damping factor of 0.0002 was employed.

2.2 Validation results

The FE predicted and experimentally obtained failure temperatures, θ_{FE} and θ_{Test}, respectively of the modelled carbon steel frames are presented in Table 2. These temperatures both refer to the temperature corresponding to the beam vertical deflection of $L/60$, where L is the frame width. The ratio of the predicted-to-measured failure temperature ranged from 0.96 to 1.11 except for the EHR5 specimen, where this ratio was greater 1.18. It was reported by the authors in [20] that the EHR5 frame was in the plastic range prior to undergoing elevated temperatures. The mean and the coefficient of variation (COV) of the FE-to-test critical temperature were 1.035 and 0.055, respectively. Figures 2(a) and (b) show the FE and test displacement-temperature responses of the EHR3 and ZSR1 frames, respectively. The trend of the increase in the predicted displacements with temperature agrees well with the measured results. The predictive accuracy of the developed FE models is therefore considered acceptable. Similar validation exercises conducted by the authors for stainless steel and carbon steel columns and beams of I- and hollow sections subjected to elevated temperatures [18-19, 23] resulted similar levels of accuracy. Hence, the described modelling approach may reliably be used for the parametric numerical modelling investigation of stainless steel frames at elevated temperatures.

3. Parametric study models

3.1 Investigated parameters

The numerical parametric modelling was conducted to study the structural performance of stainless steel frames in fire and make comparative analysis with carbon steel frames. The stainless steel frames were of austenitic EN 1.4301 and EN 1.4571 grades and the carbon steel frame was S275. The geometry and loading configuration of the modelled frames are shown in Figure 3. The frame members were all hot-finished RHS 180×100×8 cross-sections, classified as Class 1 according to the EN 1993-1-4 cross-section classification limits [1].

For each stainless steel grade, two series of frames, namely sway and non-sway frames, were considered in the parametric study. In EN 1993-1-1 [24], the elastic buckling load factor α_{cr}, defined as the ratio of the elastic critical buckling load P_{cr} to the applied design load P_{Ed} is used to classify sway and non-sway type frames. For plastic collapse analysis, these limits are $P_{cr}/P_{Ed} \geq 15$ for non-sway frames and $P_{cr}/P_{Ed} < 15$ for sway frames. Sway and non-sway type frames were achieved through the different applied load combinations on the modelled frames. The sway frames had an applied total vertical ($q \times L$) to horizontal (P) load ratio of 12, giving an elastic buckling load factor of $\alpha_{cr} = 6.1$ and 6.8 for the stainless steel (both EN 1.4301 and EN 1.4571) and carbon steel models, respectively. For the non-sway frame this load ratio was 1 with the elastic buckling load factor of $\alpha_{cr} = 19.5$ for stainless steel and 23.9 for carbon steel. The elastic critical buckling loads P_{cr} were determined by conducting a linear eigenvalue buckling analysis of the frames subjected to the applied loading conditions at room temperature and taking the eigenvalue corresponding to the lowest sway buckling mode. The applied design loads P_{Ed} of the frames were determined by conducting a geometrically and materially nonlinear stress analysis with imperfections at room temperature which are reported in Table 3. Using a first order plastic analysis, the sway frames were designed to form a 'global failure mechanism', where the overall strength of the frames is tested, involving the strength of the column and the beam, whereas the non-sway frames were designed to form the so-called 'sway failure mechanism', where only the column resistance is tested. The predicted plastic collapse loads P_{pl} of the frames are reported in Table 3.

The modelled frames were subjected to a range of degrees of utilization μ_0 of 0.2, 0.3, 0.4, 0.5, 0.6 and 0.7, where μ_0 is the ratio of the applied loading on the frames i.e. P or q at elevated temperature to their load-bearing capacities at room temperature i.e. P_u (=P_{Ed}) or q_u,

respectively. Two heating profiles were considered, including heating of all the four sides of the frame members and heating of the three interior sides of the frame members only as shown in Figure 3. In total 72 frames were modelled as summarised in Table 4.

3.2 Details of parametric FE models

The validated FE modelling approach described in Section 2 was adopted to simulate the thermal and mechanical response of the EN 1.4301 and EN 1.4571 stainless steel frames at elevated temperature and make comparisons with the S275 carbon steel frames. The thermal and mechanical properties of stainless steels, as described hereafter, were incorporated into the FE models. The stress-strain relationship of stainless steel at elevated temperature was described by means of the Ramberg-Osgood material model provided in the Design Manual for Stainless Steel Structures [3]. For both stainless steels considered, the room temperature material properties and the elevated temperature strength and stiffness reduction factors were obtained from [25] and [3], respectively. In the heat transfer model, the ISO-834 heating curve was adopted, and the emissivity coefficient and the convective heat transfer coefficient of stainless steel were set to 0.4 and 25 W/m²K, respectively [2].

The thermal material properties specified in the Design Manual for Structural Stainless Steel [3] were adopted. The heat transfer model included an additional feature to simulate the cavity radiation inside the box sections, defined by the *CAVITY DEFINITION interaction command in ABAQUS [21], as it was done in previous studies [26]. For initial geometric imperfections, the out-of-straightness of the beam and column members was modelled by half sine waves of amplitudes $L/1000$ and $h/1000$, respectively [27]. The initial sway imperfection $\phi = 1/200$ (i.e. frame initial out-of-straightness = $h/200$) was assumed as recommended in EN 1993-1-1 [24], which was applied in the FE models as an equivalent horizontal force. The column bases had pin-ended boundary conditions, with free rotation about the cross-section major axis. All modelled frames were restrained laterally to ensure in-plane frame behaviour.

4. Analysis of results and discussions

4.1 Definition of the failure criteria

As explained in Section 3.1 the sway frames were designed to form a ‘global failure mechanism’ (i.e. plastic hinges forming at the beam mid-span and at the beam-to-column junction) and the non-sway frames were designed to form a ‘sway failure mechanism’ (i.e.

plastic hinges forming at the beam-to-column joints). Figure 4 illustrates the frame failure mechanisms together with the deflected shape responses obtained from the FE models.

Considering the different deflected shape responses of the sway and non-sway frames, suitable failure criteria in terms of the maximum deflection reached at elevated temperature needed to be first established. EN 1363-1 [28] sets out distinct failure criteria for flexural loaded elements i.e. beams and vertically loaded elements i.e. columns in fire in terms of limiting deflection and limiting rate of deflection and limiting vertical contraction and limiting rate of vertical contraction, respectively. The EN 1363-1 limiting deflection D and limiting rate of deflection dD/dt requirements for flexural members are presented in Equations (1) and (2), respectively where L is the member length and d is the height of the cross-section.

$$D = \frac{L^2}{400 \cdot d} \text{ (mm)} \tag{1}$$

$$\frac{dD}{dt} = \frac{L^2}{9000 \cdot d} \text{ (mm/min)} \tag{2}$$

Based on the EN 1363-1 [28] performance criteria for flexural members, two sets of modified limiting deflection and limiting rate of deflection have been defined herein, one for sway frames and the other for non-sway frames, that are compatible with their observed deflected shape responses shown in Figure 4. For the sway frames, the limits relate to the vertical deflection D_v and the rate of vertical deflection dD_v/dt given by Equations (3) and (4), respectively, where L is taken as the frame width. For the non-sway frames, the limits are in term of the horizontal deflection D_h and the rate of horizontal deflection dD_h/dt given by Equations (5) and (6), respectively, where h is taken as the frame height. The definitions of deflections D_v and D_h are illustrated in Figure 4. The horizontal deflection limit D_h has been doubled because the horizontal deflection is measured at the top of the column and not at mid-height.

The deflection rates were observed to be highly dependent on the degree of utilisation μ_0, with frames with higher degrees of utilisation ratio showing higher deflection rates. This is because the higher the degree of utilisation the lower the time fire resistance becomes, and hence the time elapsed to describe similar displacements is shorter. Therefore, applying the same deflection rate limit to frames with different degrees of utilisation seemed unfair and the comparison between them would not be accurate. To solve this, and in order to not further

reduce the displacement limit, the normalised degree of utilisation $10\mu_0$ has been included in the definitions of the deflection rate limit in Equations (4) and (6), giving higher deflection rate limits for higher degrees of utilisation. This allowed a more realistic comparison of the failure temperatures across the range of utilisation ratios to be achieved.

For sway frames:

$$D_v = \frac{L^2}{400 \cdot d} \text{ (mm)} \tag{3}$$

$$\frac{dD_v}{dt} = \frac{L^2}{9000 \cdot d} \cdot 10\mu_0 \text{ (mm/min)} \tag{4}$$

For non-sway frames:

$$D_h = 2\frac{h^2}{400 \cdot d} \text{ (mm)} \tag{5}$$

$$\frac{dD_h}{dt} = \frac{h^2}{9000 \cdot d} \cdot 10\mu_0 \text{ (mm/min)} \tag{6}$$

In this study, failure to support the applied loads was deemed to have occurred when both criteria i.e. Equations (3) and (4) for sway frames and Equations (5) and (6) for non-sway frames have been exceeded. The suitability of the presented failure criteria has been assessed against the validation frames. The critical temperature of the EGR, EHR and ZGR frames tested by Rubert and Schaumann [20] has been obtained according to the failure criteria established in Equations (3) to (6). The obtained results are shown in Table 5 and exhibit good agreement with the critical temperatures obtained by Rubert and Schaumann [20], reinforcing the suitability of the failure criteria presented.

The time t and temperature θ corresponding to both the deflection and the rate of deflection limits of the parametric study frames were determined and are reported in Table 6. In Table 6, the failure time and temperature values, corresponding to where both criteria have been exceeded, are presented in bold. Table 7 shows the ultimate displacement achieved for the modelled frames corresponding to the criterion governing the frame failure. For the frames that are subjected to fire on three sides of the cross-section, the failure temperature is the average temperature of the cross-section corresponding to the specified failure time.

4.2 Effect of the non-uniform heating on the frame response

The temperature field of the studied frames were obtained from the heat transfer analysis models. The thermal response depends on the thermal properties of the material, the cross-section geometry and the heating profile i.e. heating on four sides or three interior sides of the frame members. Figure 5 shows the time-temperature response of the carbon steel and stainless steel frames during the first 40 minutes of fire exposure in terms of (a) the average temperature and (b) the maximum temperature of the cross-section. As both stainless steel grades, EN 1.4301 and EN 1.4571, have the same thermal properties, as specified in [3], their temperature development is identical. Figure 5 shows that the carbon steel frames gain temperature at a faster rate than the stainless steel frames at early stages of fire, but when carbon steel undergoes a phase change over the 750 ºC-780 ºC temperature, the specific heat of the material increases very abruptly, thereby making both frames to have a similar temperature henceforth. The temperature gradient for the frames subjected to fire on three interior sides may also be observed in Figure 5, where there is a difference between the average and the maximum temperature of the cross-section. Since the maximum temperature of these frames do not show the real temperature of the cross-section, the average temperature is used in all the analysis performed herein. Also, as expected, there is a temperature difference between the frames subject to fire on all four sides and the frames subject to fire on the three interior sides, which is larger at the early stages of fire and smaller at higher temperatures.

Figure 6 shows the time-displacement and temperature-displacement responses of the EN 1.4571 stainless steel frames subjected to heating on four sides and three interior sides, where the time and temperature fire resistances have been marked with an asterisk (*). Prior to the start of runaway deflections at high temperatures, the frames with heating on three side show larger vertical and horizontal deflections than the frames with heating on four side. This could be due to the additional bending moments generated in the cross-section of the frame members by the temperature gradient across the depth of the cross-section. At high temperatures, when the temperature distributions become more uniform across the cross-section, frames with both heating profiles show similar responses. The different heating profiles however resulted in a slight difference in the time t and temperature θ fire resistances of the frames, with the frames with heating on three interior sides having marginally lower failure temperature θ, due to the additional bending stresses, but higher failure time t, due to the slower heating up rate – see Table 6. For other types of structures where the imposed thermal displacements are restrained,

internal forces and bending moments are induced and should be considered in checking the overall structure and its elements. If these additional internal forces and bending moments are not considered in the structural fire design, the designed structure may collapse earlier than expected.

4.3 Sway and non-sway frames

The sway and non-sway frames were designed to form 'global failure mechanism' and 'sway failure mechanism', respectively; these failure modes were observed for all the modelled frames. Figure 7 compares the temperature-displacement response of the EN 1.4301 stainless steel sway and non-sway frames. For both frames the vertical displacement is initially downwards due to the applied load at room temperature, which starts to reduce as the temperature increases and the beam member starts to expand. At high temperatures, the increasing downward mechanical deflection, which is controlled by the reducing elevated temperature material stiffness, overtakes the thermal expansion and the deflection starts to runaway until the applied load can no longer be sustained, and the frame failure mechanisms are formed. Figure 8 shows the variation of the time t and temperature θ at failure of the modelled frames, determined in accordance with the criteria set out in Section 4.1, with the degree of utilisation μ_0. The data presented in Figure 8 belong to the frames with heating on 3 and 4 sides, both exhibiting very similar responses. As expected, the time and temperature at failure reduce with increasing degree of utilisation for both sway and non-sway frames and both stainless steel and carbon steel materials. For a given degree of utilisation, the non-sway frames showed lower failure time and temperature than the sway frames for both carbon steel and stainless steel. This is due to the ability of the analysed sway frames to form a complete failure mechanism that utilises the resistance of the whole frame, involving the resistance of both the beam and the column, giving them a higher capacity of redistributing internal forces while the non-sway frames fail by forming the so-called sway mechanism that only involves the column resistance.

4.4 Carbon steel and stainless steel

The time-displacement and temperature-displacement of the carbon steel and stainless steel non-sway frames are shown in Figure 9 and those for sway frames are shown in Figure 10, where both carbon steel and stainless steel are shown to have similar response trends. The ratios of the stainless steel-to-carbon steel time at failure (t_{ss}/t_{cs}) and temperature at failure (θ_{ss}/θ_{cs})

for all the modelled frames are presented in Table 8. Both stainless steel grades generally show higher time and temperature fire resistances than the carbon steel frames. This is due to the combination of (1) the lower heating up rate of stainless steel (2) the different elevated temperature stress-strain behaviours of the materials and (3) the higher retention of strength and stiffness of stainless steel over the important temperature range of 550-750 ºC – see Figure 11. The carbon steel frames with high utilisation ratios, $\mu_0 \geq 0.6$, however seem to have improved fire resistance than the EN 1.4301 stainless steel frames. This is due to the fact that carbon steel does not lose its yield stress until 400 ºC, whereas both the yield stress and the ultimate tensile stress of stainless steel start to reduce from 100 ºC – see Figure 11. As a result, for high degrees of utilisation, where the critical temperature is usually lower, the carbon steel frames may perform better under certain fire scenarios. The EN 1.4571 stainless steel frames have the highest time and temperature fire resistances for all degrees of utilisation, which is expected due to their superior elevated temperature strength and stiffness as shown in Figure 11.

Figure 12 shows the failure temperature θ of the frames with different utilisation ratios μ_0. The reduction factor for the 0.2% proof stress $k_{0.2}$ and the effective yield strength k_y for S275 carbon steel from [2] and the 0.2% proof stress $k_{0.2}$ and the ultimate tensile stress k_u for EN 1.4301 and EN 1.4571 stainless steels from [3] are also depicted in Figure 12. The failure temperature data for each of the materials follow the same trend as of their strength reduction factors. The failure temperatures appear to follow the reduction factor for effective yield stress k_y for the carbon steel frames and the reduction factors for the ultimate tensile stress k_u for the stainless steel frames, suggesting that frame collapse is ruled by the effective yield stress for the carbon steel frames and the ultimate tensile stress for the stainless steel frames. Therefore, the analysed frames are forming the complete plastic failure mechanism for all degrees of utilisation before collapsing and using up all the resistance provided by the material and the frame design. For design purposes, provided that the frame members are not prone to premature failure by buckling instabilities, the utilisation ratio together with the strength reduction factors may be used to obtain an initial estimate of the failure temperature of the frame assembly.

5. Conclusions

A comprehensive computational study was carried out to investigate the structural performance of stainless steel two-dimensional frames at elevated temperatures. Validated thermal and

mechanical numerical models capable of simulating, with high predictive accuracy, the full load-deformation history of two-dimensional steel frame assemblies at elevated temperature were generated. The effect of key behavioural parameters including frame type, i.e. sway and non-sway, degree of utilisation, material grade and heating profile was investigated through an extensive parametric modelling, which were analysed and discussed. Based on the analysis, for the considered tubular frame assemblies, the following conclusions can be drawn:

- The proposed performance criteria, in terms of the limiting deflection and limiting rate of deflection, for sway and non-sway frames provide a rigorous method for determining the failure time and temperature at elevated temperature.
- The different heating profiles of the frames were found to result in a slight differences in the time t and temperature θ at failure, with the frames with heating on three interior sides having marginally lower failure temperature θ, due to the additional bending stresses, but higher failure time t, due to the slower heating up rate.
- The time and temperature at failure were found to reduce with increasing degree of utilisation for both sway and non-sway frames and both stainless steel and carbon steel materials. For a given degree of utilisation, the non-sway frames showed lower failure time and temperature than the sway frames for both carbon steel and stainless steel. This is due to the ability of the sway frames to utilise the resistance of the whole frame, involving the resistance of the beam and the column, giving them a higher capacity of redistributing internal forces.
- Both stainless steel grades considered generally showed higher time and temperature fire resistances than the carbon steel frames, which is due to the combination of (1) the lower heating up rate of stainless steel and (2) the higher retention of strength and stiffness of stainless steel over the important temperature range of 550-750 ºC
- The variation of the failure temperatures and utilisation ratios of the studied frames appeared to follow the reduction factors for yield stress k_y for the carbon steel frames and the reduction factors for the ultimate tensile stress k_u for the stainless steel frames. It was suggested that for design purposes, provided that the frame members are not prone to premature failure by buckling instabilities, the utilisation ratio together with the strength reduction factors may be used to obtain an initial estimate of the failure temperature of the frame assembly.

Acknowledgements

The first author acknowledges the support of the Secretaria d'Universitats i Recerca de la Generalitat de Catalunya (Spain) and the European Social Fund. The authors acknowledge the funding from the MINECO (Spain) under Project BIA2016-75678-R, AEI/FEDER, UE "Comportamiento estructural de pórticos de acero inoxidable. Seguridad frente a acciones accidentales de sismo y fuego".

References

[1] European Committee for Standardization (CEN). *EN 1993-1-4:2006. Eurocode 3: Design of Steel Structures – Part 1-4: General Rules. Supplementary Rules for Stainless Steels.* Brussels, Belgium, 2006.

[2] European Committee for Standardization (CEN). *EN 1993-1-2:2005. Eurocode 3: Design of Steel Structures – Part 1-2: General Rules. Structural fire design*. Brussels, Belgium, 2005.

[3] Design Manual of Structural Stainless Steel. 4th Edition. Ascot, United Kingdom, 2017. ISBN: 978-1-85942-226-7.

[4] Usmani A. S.; Rotter J. M.; Lamont S.; Sanad A. M.; Gillie M. *Fundamental principles of structural behaviour under thermal effects*. Fire Safety Journal, 36(8), 721-744, 2001.

[5] Lamont S.; Lane B.; Flint G.; Usmani *A. Behaviour of structures in fire and real design – A case study*. Journal of Fire Protection Engineering, 16, 5-35, 2006.

[6] Gillie M.; Usmani A. S.; Rotter J. M. *A structural analysis of the first Cardington test*. Journal of Constructional Steel Research, 57(6), 581-601, 2001.

[7] Ng, K.T.; Gardner, L. *Buckling of stainless steel columns and beams in fire*. Engineering Structures, 29(5), 717-730, 2007.

[8] Fan, S.; He, B.; Xia, X.; Gui, H.; Liu, M. *Fire resistance of stainless steel beams with rectangular hollow section: Experimental investigation*. Fire Safety Journal, 81, 17-31, 2016.

[9] Fan, S.; Chen, G.; Xia, X.; Ding, Z.; Liu, M. *Fire resistance of stainless steel beams with rectangular hollow section: Numerical investigation and design*. Fire Safety Journal, 79, 69-90, 2016.

[10] Uppfeldt, B.; Ala Outinen, T.; Veljkovic, M. *A design model for stainless steel box columns in fire*. Journal of Constructional Steel Research, 64, 1294-1301, 2008.

[11] Tondini, N.; Rossi, B.; Franssen, J.M. *Experimental investigation on ferritic stainless steel columns in fire*. Fire Safety Journal, 62, 238-248, 2013.

[12] Huang, Y.; Young, B. *Finite element analysis of cold-formed lean duplex stainless steel columns at elevated temperatures*. Thin-Walled Structures, 143, 106203, 2019.

[13] Fan, S.; Zhang, L.; Sun, W.; Ding, X.; Liu, M. *Numerical investigation on fire resistance of stainless steel columns with square hollow section under axial compression*. Thin-Walled Structures, 98, 185-195, 2016.

[14] Lopes, N.; Vila Real, P.; da Silva, L.S.; Franssen, J.M. *Numerical analysis of stainless steel beam-columns in case of fire*. Fire Safety Journal, 50, 35-50, 2012.

[15] Lopes, N.; Manuel, M.; Sousa, A.R.; Vila Real, P. *Parametric study on austenitic stainless steel beam-columns with hollow sections under fire*. Journal of Constructional Steel Research, 152, 274-283, 2019.

[16] Fan, S.; Li, Y.; Li, Z.; Liu, M.; Han, Y. *Experimental investigation of fire resistance of axially compressed stainless steel columns with constraints*. Thin-Walled Structures, 120, 46-59, 2017.

[17] Rodrigues, J.P.; Laím, L. *Comparing fire behaviour of restrained hollow stainless steel with carbon steel columns*. Journal of Constructional Steel Research, 153, 449-458, 2019.

[18] Pournaghshband, A.; Afshan, S.; Theofanous, M. *Elevated temperature performance of restrained stainless steel beams*. Structures, 22, 278-290, 2019.

[19] Pournaghshband, A.; Afshan, S.; Foster, A.S.J. *Structural fire performance of axially and rotationally restrained stainless steel columns*. Thin-Walled Structures, 137, 561-572, 2019.

[20] Rubert, A.; Schaumann, P. *Structural Steel and Plane Frame Assemblies under Fire Action*. Fire Safety Journal, 10, 173-184, 1986.

[21] Abaqus Documentation. Abaqus 2016. Abaqus, Version 6.16. Dassault Systmes Simulia Corp. USA.

[22] Jiang, J. *Nonlinear thermomechanical analysis of structures using OpenSees*. PhD thesis, The University of Edinburg, 2013.

[23] Mohammed, A.; Afshan, S. *Numerical modelling and fire design of stainless steel hollow section columns*. Thin-Walled Structures, 144, 106243, 2019.

[24] European Committee for Standardization (CEN). *EN 1993-1-1. Eurocode 3 – Design of Steel Structures – Part 1-1: General rules and rules for buildings*. Final Document. Brussels, Belgium, 2005.

[25] Afshan, S.; Zhao, O.; Gardner, L. *Standardised material properties for numerical parametric studies of stainless steel structures and buckling curves for tubular columns.* Journal of Constructional Steel Research, 152, 2-11, 2019.

[26] Segura, G.; Afshan, S.; Mirambell, E.; Real. E. *Numerical analysis of stainless steel frames subject to fire.* Congress on Numerical Methods in Engineering 2019, CMN19. Guimaraes, Portugal, 2019.

[27] European Committee for Standardization (CEN). *EN 1993-1-5:2004. Eurocode 3 – Design of Steel Structures – Part 1-5: Plated structural elements*. Final Document. Brussels, Belgium, 2004.

[28] European Committee for Standardization (CEN). *EN 1363-1:2020. Fire resistance tests – Part 1: General Requirements.* Brussels, Belgium, 2020.

Table 1: Key details of the tested frames from [20].

Frame	L (mm)	h (mm)	F_1 (kN)	F_2 (kN)	μ_0	θ (°C)	f_y (N/mm^2)	Remarks	
EHR1	1190	1170	56	14	0.38	600	395	Major axis bending	All members fully heated
EHR2	1240	1170	84	21	0.59	530	395		
EHR3	1240	1170	112	28	0.82	475	382		
EHR4	1250	1500	20	5	0.59	562	389	Minor axis bending	
EHR5	1250	1500	24	6	0.71	460	389		
EHR6	1250	1500	27	6.7	0.79	523	389		
EGR1b	1220	1170	65	2.5	0.55	533	382	Major axis bending	All members fully heated
EGR1c	1220	1170	65	2.5	0.55	515	382		
EGR2	1220	1170	40	1.6	0.34	612	385		
EGR3	1220	1170	77	3.0	0.66	388	385		
EGR4	1220	1170	77	3.0	0.63	424	412		
EGR5	1220	1170	88	3.4	0.72	335	412		
EGR6	1220	1170	88	3.4	0.72	350	412		
EGR7	1220	1170	68.5	2.6	0.65	454	320		Cold beam
EGR8	1220	1170	77	3.0	0.70	464	385		
ZSR1	1200	1180	74.0	2.9	0.60	547	355	Major axis bending	Partly heated
ZSR2	1200	1180	84.5	3.3	0.66	479	380		
ZSR3	1200	1180	68.5	68.5	0.50	574	432		

Table 2: FE and test critical temperatures.

Frame	θ_{FE} (°C)	θ_{Test} (°C)	$\theta_{FE}/\theta_{Test}$
EHR1	627	600	1.04
EHR2	559	530	1.06
EHR3	474	475	1.00
EHR4	578	562	1.03
EHR5	545	460	1.18
EHR6	522	523	1.00
EGR1b	509	533	0.96
EGR1c	509	515	0.99
EGR2	600	612	0.98
EGR3	425	388	1.10
EGR4	445	424	1.05
EGR5	371	335	1.11
EGR6	371	350	1.06
EGR7	456	454	1.00
EGR8	453	464	0.98
ZSR1	542	547	0.99
ZSR2	507	479	1.06
ZSR3	600	574	1.05

Table 3: P_{Ed}, P_{cr}, P_{pl} of the modelled frames at room temperature.

Steel grade	Frame type	P_{Ed} (kN)	P_{cr} (kN)	P_{pl} (kN)	P_{cr}/P_{Ed}
EN 1.4301	Sway	11.6	70.9	10.5	6.1
	Non-sway	41.4	807.2	37.4	19.5
EN 1.4571	Sway	11.6	70.9	10.5	6.1
	Non-sway	41.4	807.2	37.4	19.5
S275	Sway	11.0	74.4	10.3	6.8
	Non-sway	35.4	847.6	36.7	23.9

Table 4: Summary of investigated parameters.

Steel grade	Frame type	Heating	degree of
EN 1.4301	Sway and non-sway	3 sides, 4 sides	0.2, 0.3, 0.4, 0.5, 0.6 and 0.7
EN 1.4571	Sway and non-sway	3 sides, 4 sides	0.2, 0.3, 0.4, 0.5, 0.6 and 0.7
S275	Sway and non-sway	3 sides, 4 sides	0.2, 0.3, 0.4, 0.5, 0.6 and 0.7

Table 5: Critical temperatures of the validation frames obtained from applying the defined failure criteria θ_{FE} and compared to the test critical temperatures θ_{Test}.

Frame	μ_0	D_v (mm)	dD_v/dt (mm/min)	D_h (mm)	dD_h/dt (mm/min)	θ_{FE} (°C)	θ_{Test} (°C)	$\theta_{FE}/\theta_{Test}$
EHR1	0.38	88.5	486.8	42.8*	470.6	637	600	0.95
EHR2	0.59	96.1	528.6	42.8*	470.6	566	530	0.98
EHR3	0.82	96.1	326.7	42.8*	290.9	489	475	0.97
EHR4	0.59	97.7	644.5	140.6	928.1	639	562	1.09
EHR5	0.71	97.7	615.2	140.6	885.9	615	460	1.04
EHR6	0.79	97.7	703.1	140.6	1012.5	598	523	1.09
EGR1b	0.55	93.0	669.8	85.6	616.0	506	533	1.05
EGR1c	0.55	93.0	604.7	85.6	556.1	506	515	0.99
EGR2	0.34	93.0	651.2	85.6	598.9	596	612	0.97
EGR3	0.66	93.0	353.5	85.6	162.6	421	388	1.06
EGR4	0.63	93.0	548.8	85.6	252.4	441	424	1.07
EGR5	0.72	93.0	762.8	85.6	350.8	366	335	1.03
EGR6	0.72	93.0	548.8	85.6	504.8	366	350	1.14
EGR7	0.65	93.0	660.5	85.6	607.4	450	454	1.34
EGR8	0.70	93.0	734.9	85.6	675.9	449	464	1.14
ZSR1	0.60	90.0	540.0	87.0	522.2	506	547	0.93
ZSR2	0.66	90.0	594.0	87.0	574.4	450	479	0.94
ZSR3	0.50	90.0	450.0	87.0	435.1	574	574	1.00

* The horizontal deflection limit (D_h) is measured at the middle of the column due to their failure mechanism. Therefore, the limit has not been doubled for these models as shown in Eq (5).

Table 6: Failure times t (min) and temperatures θ (ºC) of the modelled frames corresponding to the deflection D (mm) and the rate of deflection dD/dt (mm/min) criteria.

Steel grade	μ_0	Sway, 3 sides				Sway, 4 sides				Non-sway, 3 sides				Non-sway, 4 sides			
		D_v		dD_v/dt		D_v		dD_v/dt		D_h		dD_h/dt		D_h		dD_h/dt	
		t	θ	t	θ	t	θ	t	θ	t	θ	t	θ	t	θ	t	θ
S275	0.2	**34**	**789**	31	758	**32**	**793**	29	757	**30**	**742**	20	667	**28**	**746**	16	645
	0.3	**26**	**718**	23	702	**22**	**717**	19	689	**22**	**687**	18	631	**21**	**710**	15	610
	0.4	**21**	**679**	20	654	**19**	**688**	17	655	**18**	**630**	17	599	**18**	**674**	14	583
	0.5	**19**	**641**	18	612	**17**	**656**	16	628	**16**	**572**	15	564	**16**	**633**	13	570
	0.6	**17**	**600**	16	569	**15**	**624**	14	591	14	515	**14**	**535**	**14**	**593**	12	539
	0.7	**15**	**557**	14	529	**14**	**594**	13	570	12	449	**13**	**509**	**13**	**548**	12	522
EN 1.4301	0.2	**60**	**931**	59	926	**60**	**937**	58	929	43	866	**46**	**882**	**51**	**908**	43	880
	0.3	**43**	**868**	43	864	**42**	**875**	41	870	29	758	**33**	**800**	**34**	**834**	29	798
	0.4	**34**	**808**	24	807	**32**	**824**	32	819	15	467	**28**	**740**	**26**	**765**	24	737
	0.5	26	720	**27**	**735**	**26**	**771**	26	771	11	339	**24**	**683**	19	654	**20**	**676**
	0.6	20	593	**22**	**640**	21	696	**22**	**710**	8	261	**18**	**562**	12	460	**15**	**560**
	0.7	15	467	**17**	**526**	15	563	**17**	**615**	7	199	**14**	**448**	8	285	**11**	**404**
EN 1.4571	0.2	102	1017	**103**	**1020**	102	1019	**102**	**1020**	77	973	**84**	**987**	**84**	**990**	82	985
	0.3	71	960	**73**	**963**	71	963	**72**	**965**	47	883	**61**	**933**	57	926	**58**	**930**
	0.4	53	909	**55**	**916**	54	917	**55**	**920**	31	777	**47**	**884**	42	877	**44**	**882**
	0.5	42	861	**42**	**862**	43	878	**43**	**881**	14	444	**39**	**842**	33	826	**35**	**842**
	0.6	**31**	**775**	31	772	**33**	**828**	32	823	10	329	**32**	**787**	23	725	**30**	**805**
	0.7	22	638	**24**	**683**	**26**	**768**	26	767	8	252	**26**	**708**	14	529	**22**	**716**

Table 7: Ultimate displacement D_v or D_h (mm) of the modelled frames corresponding to the failure time and temperature.

Steel grade	μ_0	Sway, 3 sides	Sway, 4 sides	Non-sway, 3 sides	Non-sway, 4 sides
		D_v	D_v	D_h	D_h
S275	0.2	-500	-500	340	340
	0.3	-500	-500	340	340
	0.4	-500	-500	340	340
	0.5	-500	-500	340	340
	0.6	-500	-500	371	340
	0.7	-500	-500	424	340
EN 1.4301	0.2	-500	-500	387	340
	0.3	-500	-500	422	340
	0.4	-500	-500	524	340
	0.5	-604	-500	702	381
	0.6	-751	-611	771	469
	0.7	-781	-752	800	500
EN 1.4571	0.2	-569	-526	430	340
	0.3	-593	-554	561	375
	0.4	-651	-591	617	378
	0.5	-521	-564	701	433
	0.6	-500	-500	819	593
	0.7	-769	-500	986	640

Table 8: Ratios of failure times and temperatures of stainless steel to carbon steel frames.

Steel grade	μ_0	Sway, 3 sides		Sway, 4 sides		Non-sway, 3 sides		Non-sway, 4 sides	
		t_{ss}/t_{cs}	θ_{ss}/θ_{cs}	t_{ss}/t_{cs}	θ_{ss}/θ_{cs}	t_{ss}/t_{cs}	θ_{ss}/θ_{cs}	t_{ss}/t_{cs}	θ_{ss}/θ_{cs}
EN 1.4301	0.2	1.76	1.18	1.88	1.18	1.53	1.19	1.82	1.22
	0.3	1.65	1.21	1.91	1.22	1.50	1.16	1.62	1.17
	0.4	1.62	1.19	1.68	1.20	1.56	1.17	1.44	1.14
	0.5	1.42	1.15	1.53	1.18	1.50	1.19	1.25	1.07
	0.6	1.29	1.07	1.47	1.14	1.29	1.05	1.07	0.94
	0.7	1.13	0.94	1.21	1.04	1.08	0.88	0.85	0.74
EN 1.4571	0.2	3.03	1.29	3.19	1.29	2.80	1.33	3.00	1.33
	0.3	2.81	1.34	3.27	1.35	2.77	1.36	2.76	1.31
	0.4	2.62	1.35	2.89	1.34	2.61	1.40	2.44	1.31
	0.5	2.21	1.34	2.53	1.34	2.44	1.47	2.19	1.33
	0.6	1.82	1.29	2.20	1.33	2.29	1.47	2.14	1.36
	0.7	1.60	1.23	1.86	1.29	2.00	1.39	1.69	1.31

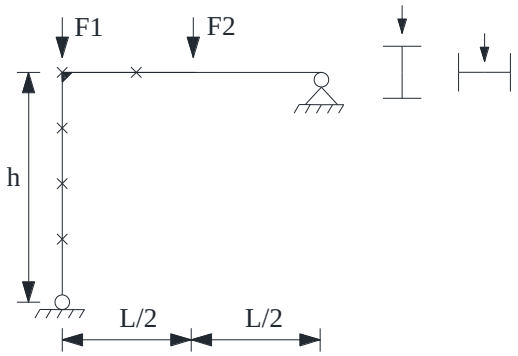

(a) Frame HER

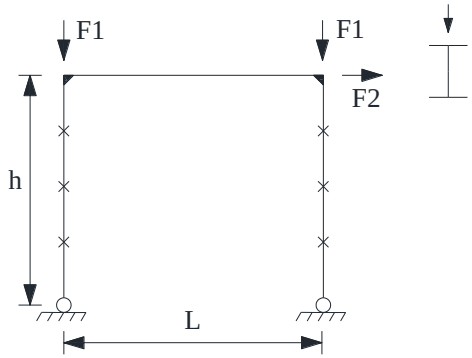

(b) Frame EGR

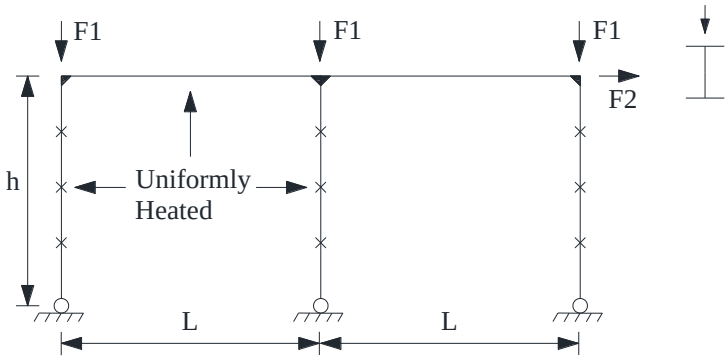

(c) Frame ZSR

Figure 1. Schematics of the carbon steel frames tested in [20] – (a) Frame HER, (b) Frame EGR and (c) Frame ZSR.

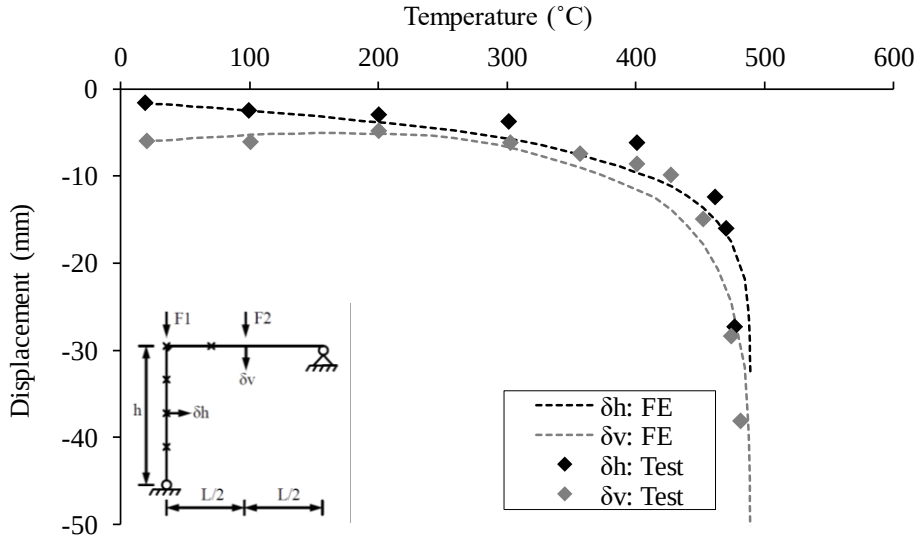

(a) Frame EHR3

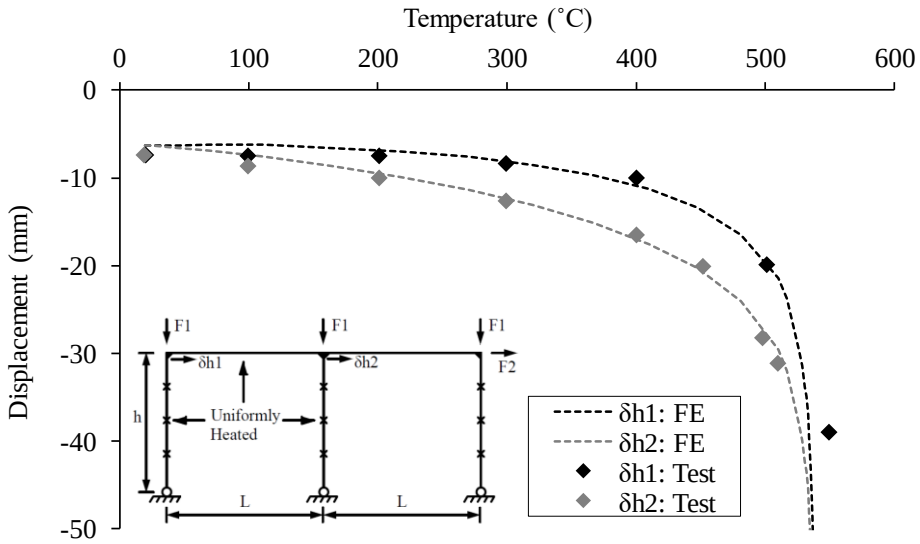

(b) Frame ZSR1

Figure 2: Comparison of displacement versus temperature responses from test and FE – (a) Frame EHR3 and (b) Frame ZSR1.

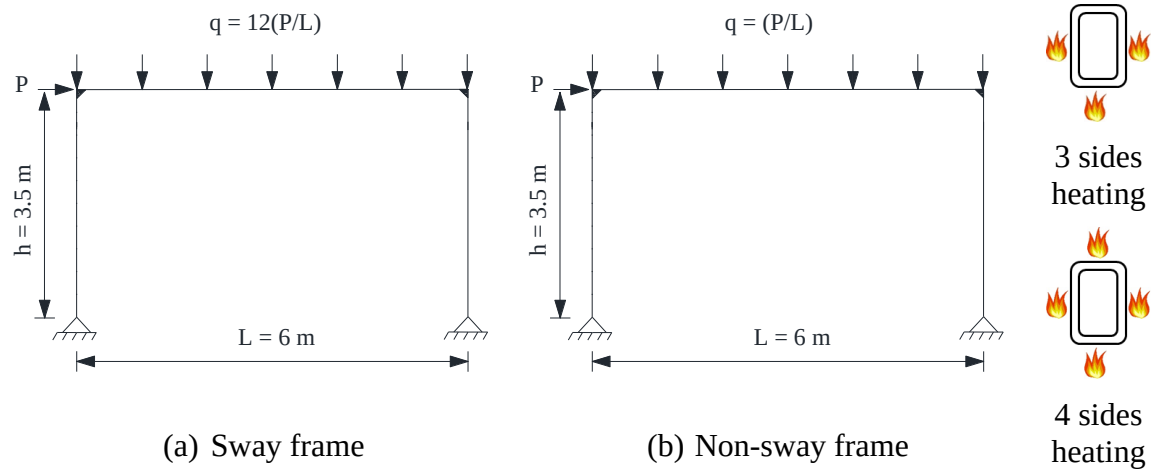

(a) Sway frame (b) Non-sway frame

Figure 3: Geometry and loading for (a) sway and (b) non-sway frames subjected to heating on 3 and 4 sides.

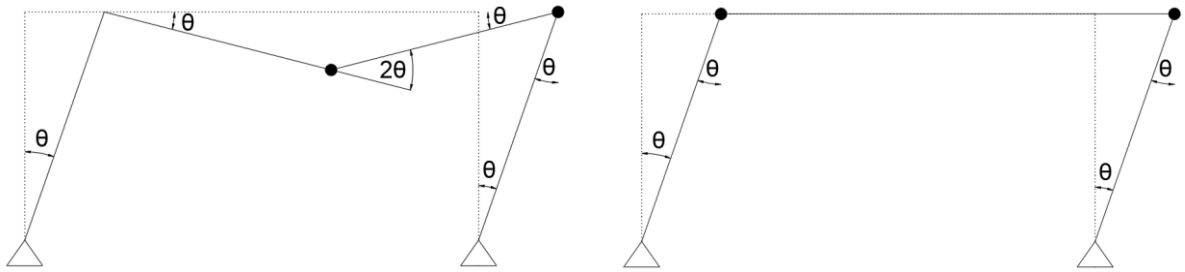

(a) Global failure mechanism (b) Sway failure mechanism

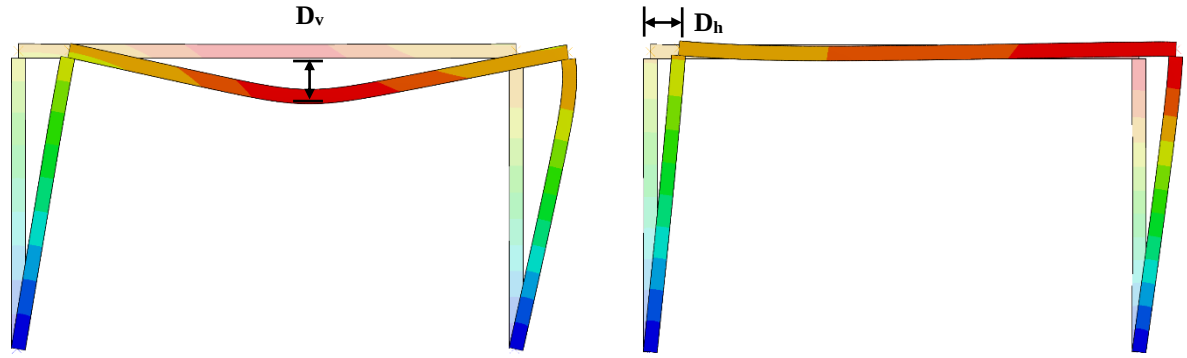

(c) FE deflected shape – Sway frame (d) FE deflected shape – Non-sway frame

Figure 4: Predicted frame failure mechanisms from first order plastic analysis and FE deflected shape responses for sway and non-sway frames.

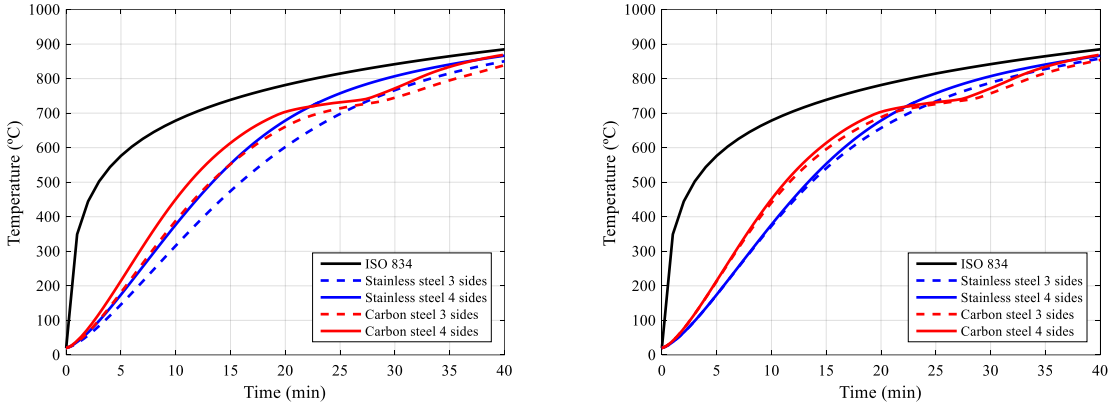

(a) Average temperature (b) Maximum temperature

Figure 5: Time-temperature development of the carbon steel and stainless steel frames – (a) average temperature and (b) maximum temperature.

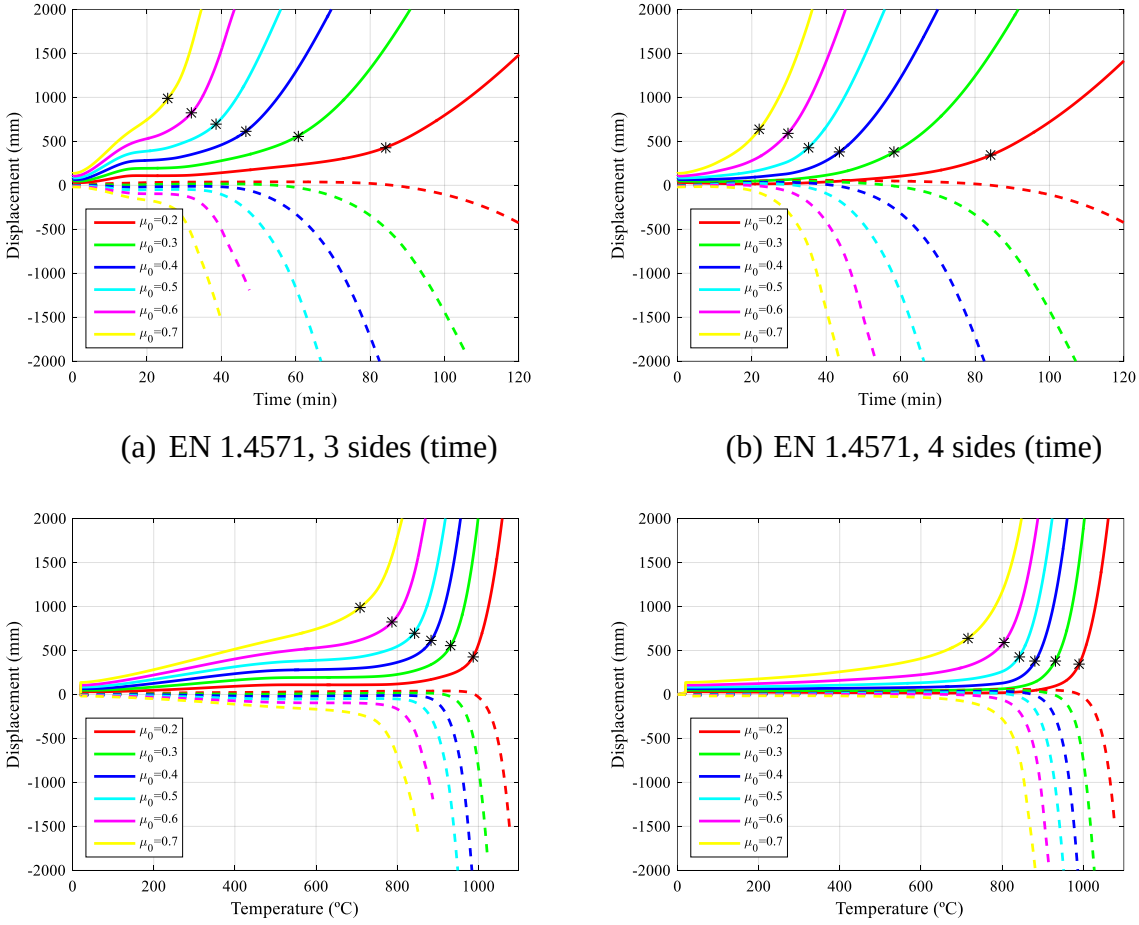

(a) EN 1.4571, 3 sides (time) (b) EN 1.4571, 4 sides (time)

(c) EN 1.4571, 3 sides (temperature) (d) EN 1.4571, 4 sides (temperature)

Figure 6: Horizontal (solid line) and vertical (dashed line) displacements versus time, (a) and (b), and temperature, (c) and (d), of EN 1.4571 stainless steel non-sway frames with 3 sides and 4 sides heating profiles.

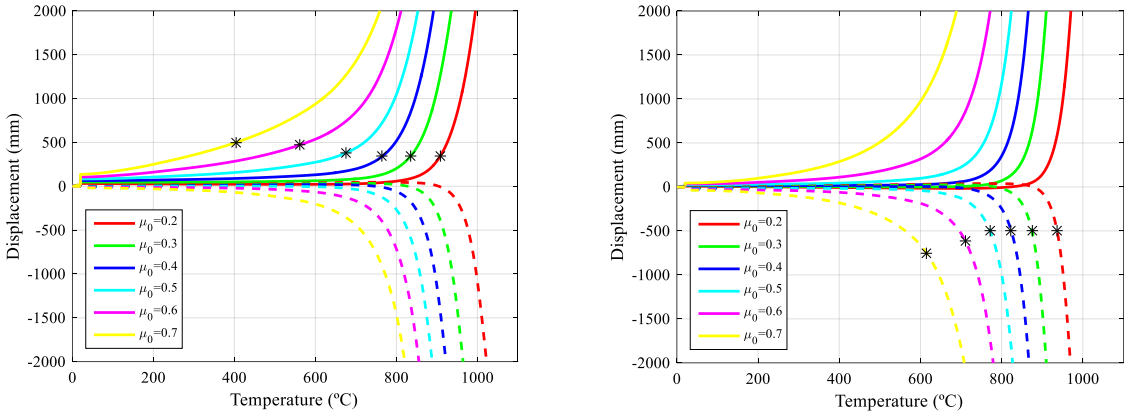

(a) EN 1.4301 – Non-sway (b) EN 1.4301 – Sway

Figure 7: Horizontal (solid line) and vertical (dashed line) displacements versus temperature for (a) Non-sway and (b) Sway EN 1.4301 stainless steel frames.

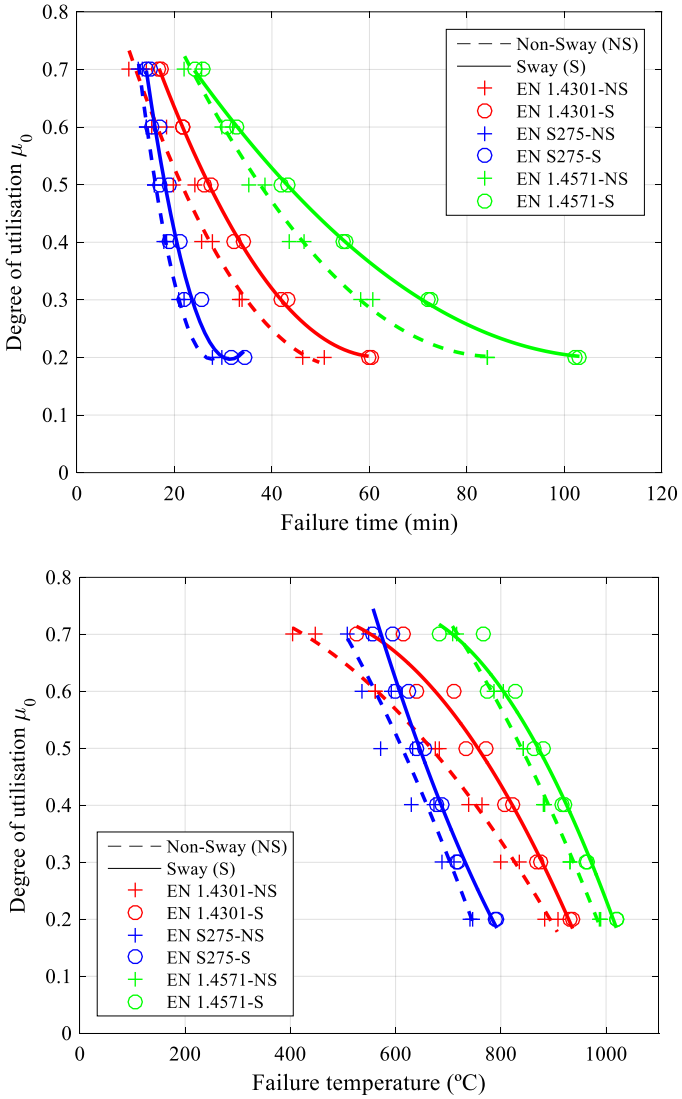

Figure 8: Variation of the time and temperature fire resistance with the degree of utilisation.

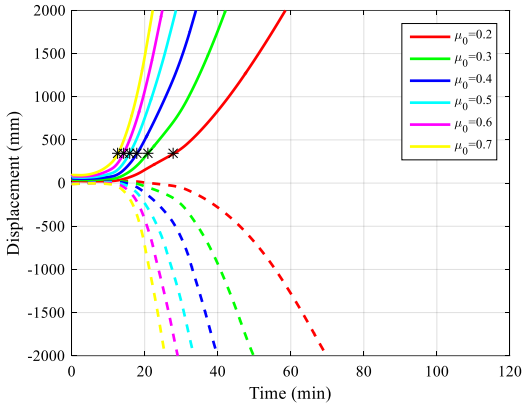

(a) S275 – Non-sway (time)

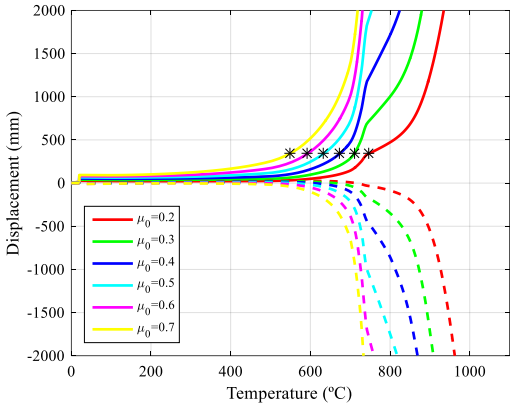

(b) S275 – Non-sway (temperature)

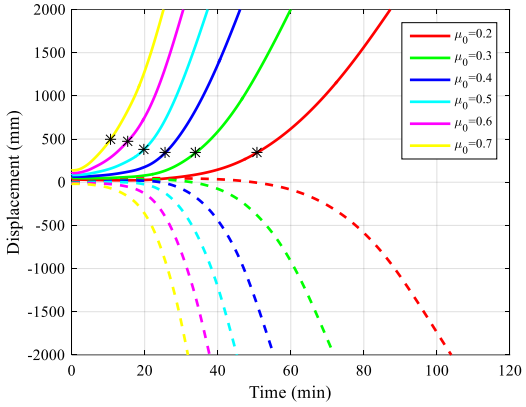

(c) EN1.4301 – Non-sway (time)

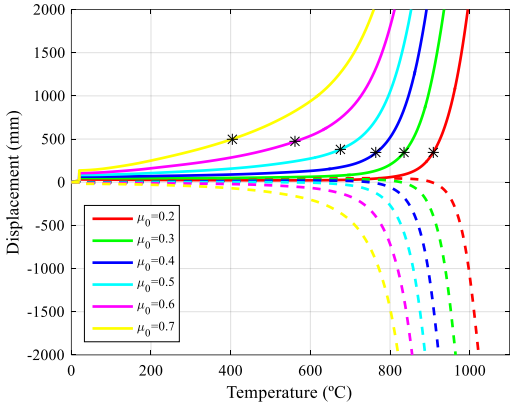

(d) EN1.4301 – Non-sway (temperature)

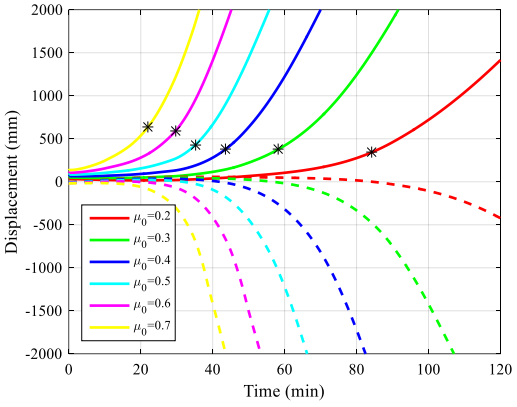

(e) EN1.4571 – Non-sway (time)

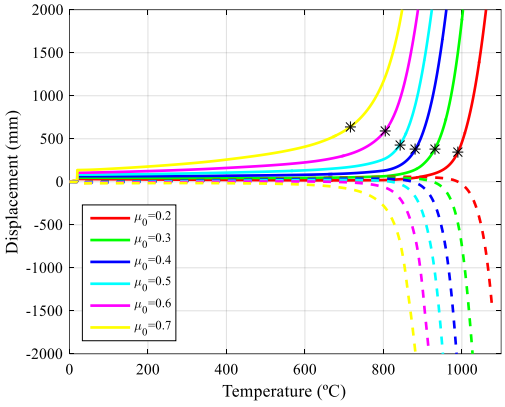

(f) EN1.4571 Non-sway (temperature)

Figure 9: Horizontal (solid line) and vertical (dashed line) displacements versus time and temperature of the non-sway frames subjected to fire on four sides – (a) and (b) for S275, (c) and (d) for EN 1.4301 and (e) and (f) for EN 1.4571.

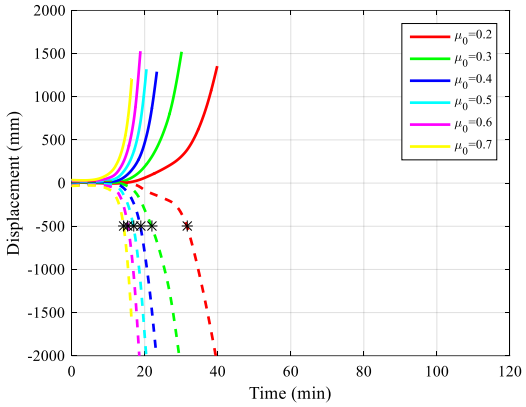

(a) S275 – Sway (time)

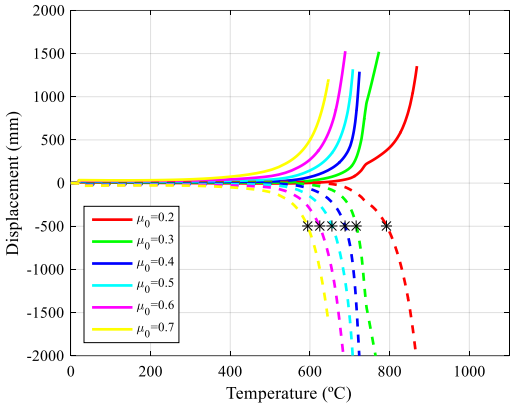

(b) S275 – Sway (temperature)

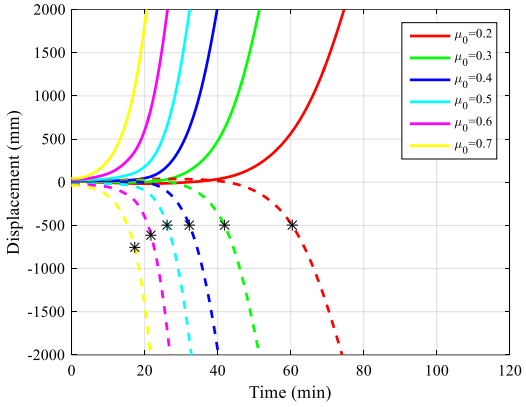

(c) EN1.4301 Sway, time

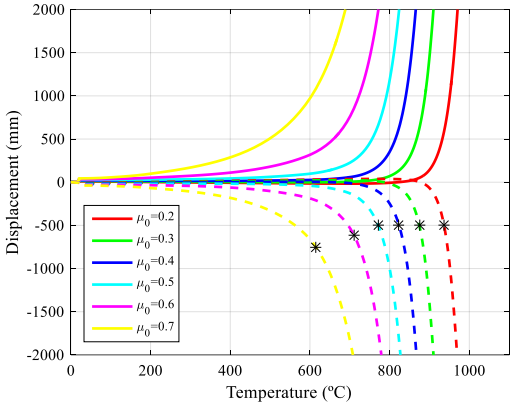

(d) EN1.4301 Sway (temperature)

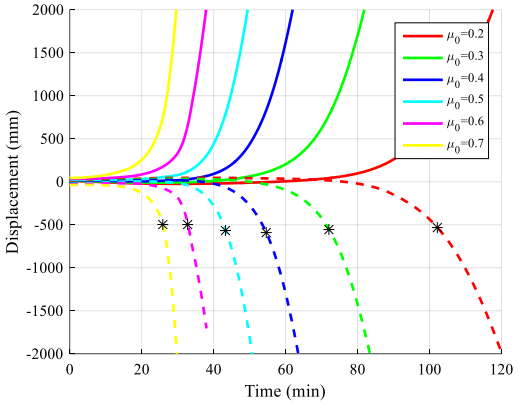

(e) EN1.4571 Sway (time)

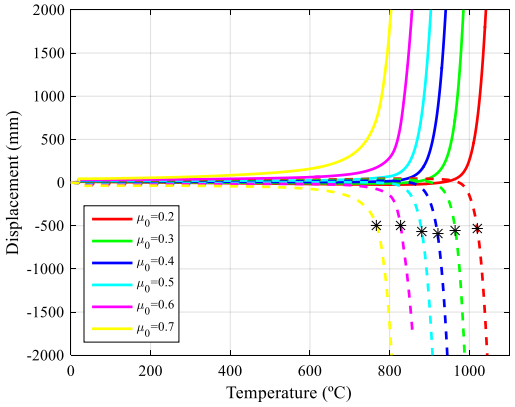

(f) EN1.4571 Sway (temperature)

Figure 10: Horizontal (solid line) and vertical (dashed line) displacements versus time and temperature of the sway frames subjected to fire on four sides – (a) and (b) for S275, (c) and (d) for EN 1.4301 and (e) and (f) for EN 1.4571.

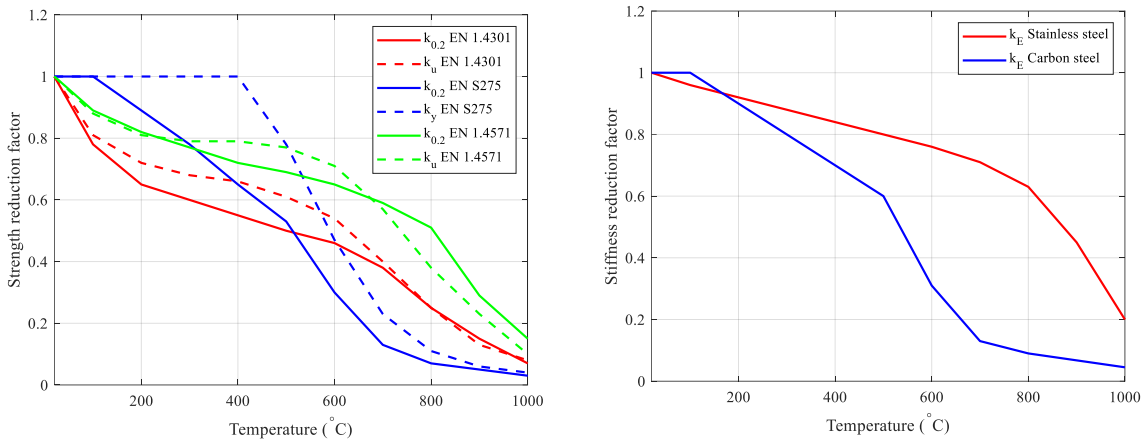

(a) Strength reduction factors (b) Stiffness reduction factors

Figure 11: Comparison of stainless steel and carbon steel elevated temperature strength and stiffness reduction factors.

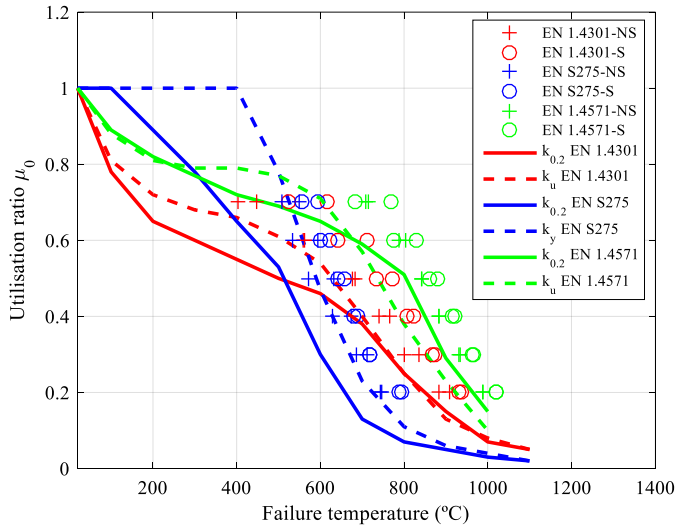

Figure 12: Comparisons between the failure temperatures of the analysed frames and the elevated temperature strength reduction factors of the materials.